

HgCdTe Photoconductive Mixers for 3-15 Terahertz

Albert Betz^a, Rita Boreiko^a, Yongdong Zhou^b, Jun Zhao^b, Yusuf Selamet^b, Yong Chang^b, Renganathan Ashokan^b, Charlie Bucker^{b,c}, and Sivalingam Sivananthan^b

^aCenter for Astrophysics & Space Astronomy, University of Colorado, Boulder, CO 80309

^bMicrophysics Laboratory & Department of Physics, University of Illinois at Chicago, IL 60607

^cPhysics Institute of Wuerzburg, Germany

ABSTRACT

We are developing HgCdTe photoconductive detectors for use as heterodyne mixers in the 3-15 THz band ($\lambda=20-100 \mu\text{m}$). These planar devices have the potential for a high quantum efficiency $\eta > 0.1$, a fast time response $\tau < 50 \text{ ps}$, a relatively low LO power requirement of $P_{\text{LO}} = 10-50 \mu\text{W}$, and an operating temperature of 10-30 K. The required thickness of the intrinsic material is $< 10 \mu\text{m}$, and so devices can be readily fabricated in array formats with planar deposition techniques.

We are using molecular-beam-epitaxy (MBE) to fabricate two types of devices for applications initially between 5-15 THz ($\lambda=20-60 \mu\text{m}$). The first device is the well-known $\text{Hg}_{1-x}\text{Cd}_x\text{Te}$ alloy, while the second is a HgTe/HgCdTe superlattice (SL) grown on either CdTe/Si or CdZnTe (112)B substrates. The bandgap of the alloy is varied by adjusting the mole fraction x of CdTe in the range of $x = 0.17-0.22$, whereas the gap of the SL depends almost entirely on the thickness of the HgTe well layers interleaved between high-gap HgCdTe barriers.

The mixers are fabricated in series of three- and six-element linear arrays. The electrical contacts are deposited on the top surface as interdigitated electrodes (IDE). In the initial test arrays, either 4-, 6-, or 8- electrode fingers of $4 \mu\text{m}$ width span the active $200 \mu\text{m}$ width of the mixer. A trade-off between response speed and mixer impedance is made by adjusting the interelectrode separation. Signal and local oscillator (LO) beams are coupled to the photomixer optically. Typically the mixer size is $3-4 \lambda$ across, so no separate antenna is required.

1. Introduction

There are 3 planar technologies currently available for fabricating photoconductors for far-infrared applications. The first is an extension of extrinsic detector technology, but with doping densities 100 times higher. Ge can be doped with Ga at densities of 10^{16} cm^{-3} , in a manner analogous to highly doped As:Si detectors. At such densities, the detector has an absorption strength of 100 cm^{-1} , and so devices only $10 \mu\text{m}$ thick should have good quantum efficiencies. Conduction in the impurity band is blocked by an undoped layer, and hence these devices are called impurity-blocked-conduction (IBC) or

blocked-impurity-band (BIB) detectors. This technology appears most promising for the 70-200 μm band, but the devices will need cooling to $T \leq 2$ K [1]. Unfortunately, inherent difficulties in handling high purity Ge compounds have made Ge-IBC devices hard to make.

The second planar technology involves the creation of quantum-well structures in III-V materials such as InAs/GaSb and others [2,3]. The quantum well devices will have absorption strengths of 100 cm^{-1} in the 10-70 μm band, and a relaxed cooling requirement of about 10 K. Theoretically, one could also make zero-band-gap III-V alloys (*e.g.*, InTlP, InTlAs, or InTlSb), but these materials have been difficult to fabricate epitaxially.

The third approach is the one favored here. It involves the II-VI group materials HgTe and CdTe, which can be used effectively in either zero-gap alloys or multiple-quantum-well (superlattice) structures [4]. Intrinsic HgTe/CdTe detectors, like extrinsic IBC devices, have minimal volumes, and hence higher radiation resistance compared to much larger extrinsic detectors with low doping. Most near-IR arrays are currently made with HgCdTe alloys, and in fact over 10^8 pixels have already been delivered by industry. This major investment by the industrial sector favors II-VI materials for either large-scale or mass-produced FIR arrays, should the technology prove applicable. Our goal is to demonstrate that II-VI technology is indeed applicable, initially between $\lambda = 40\text{-}65\ \mu\text{m}$, and later longward to $\lambda = 100\ \mu\text{m}$.

Our FIR project has 3 goals: (1) to fabricate high quality superlattice (SL) materials, (2) to fabricate discrete photoconductors and photodiodes from this material, and (3) to fabricate small linear arrays leading up to a 32×32 element direct-detection array. The array work will not be discussed further, but instead we will concentrate here on using discrete photoconductive devices as FIR heterodyne mixers. Some designs for such mixers were presented previously [5,6]. Now, two years later, we have successfully fabricated good quality SL materials and have made operating photoconductors and photodiodes for mid-infrared wavelengths. In fact, the new photodiodes are probably the first p-n junctions ever made in a II-VI superlattice material. While initial measurements are encouraging, further improvements in materials and device processing are needed before a FIR photoconductive mixer can be demonstrated.

2. Materials – Bandgap Engineering

Two approaches are available for fabricating II-VI materials with the 10-20 meV bandgaps needed for $\lambda = 50\text{-}100\ \mu\text{m}$ applications. The first is the well-known alloy approach in which the bandgap is tailored by varying the mole fraction x of CdTe in a HgCdTe alloy. This is the method used to fabricate all HgCdTe arrays to date, but none so far at FIR wavelengths. The second approach relies on the creation of a multiple quantum well structure called a superlattice (SL), in which HgTe (well) layers and CdTe (barrier) layers are alternated repeatedly. The bandgap of this composite structure is set primarily by the thickness of the well layer (HgTe). Absorption coefficients $\alpha > 1000\text{ cm}^{-1}$ are predicted for SL materials at FIR wavelengths, and so a superlattice thickness of $5\ \mu\text{m}$ should yield a 40% quantum efficiency (single pass).

2.1 Hg_{1-x}Cd_xTe Alloys

At 77 K, the band gap of the semimetal HgTe is -0.26 eV, and that of the semiconductor CdTe is 1.6 eV. These materials can be alloyed using various Cd fractions x to tune the bandgap E_g (eV) of Hg_{1-x}Cd_xTe to intermediate values (including zero) [7].

Figure 1 shows the cut-off wavelength, defined as $\lambda_c(\mu\text{m})=1.24/E_g(\text{eV})$, as a function of temperature for various fractional compositions x . It is evident that by choosing x between 0.16 and 0.17, a wide range of cut-off wavelengths in the FIR can be obtained. For the approximate 0.01 eV band gap needed for $\lambda=100 \mu\text{m}$ response, x would be close to 0.17. As the band gap approaches zero, small fractional changes in x lead to large fractional changes in the gap energy, and generally we need to control x to within 0.2% to have a 10% uncertainty in λ_c . It should be apparent that compositional gradients could lead to variations in the gap and thus a non-uniform response across an array detector. Nevertheless, we believe that by using molecular-beam-epitaxy (MBE), adequate composition control is available. As a test of this control, we successfully fabricated n-type alloy material with $x=0.165$ on silicon substrates.

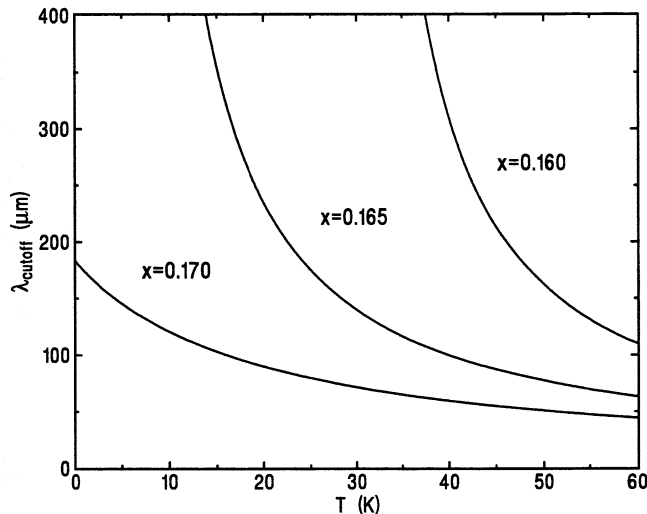


Figure 1: The cut-off wavelength is plotted against operating temperature for various Cd fractions x .

2.2 HgTe/CdTe Superlattices

A superlattice (SL) is a composite semiconductor consisting of a large number of alternating well and barrier layers – hence multiple quantum wells. HgTe/CdTe SLs form a new class called type-III SLs, because of the unique combination of a negative bandgap semimetal (HgTe) and a positive bandgap semiconductor CdTe. These layers are sequentially deposited on a CdZnSe or a CdTe/Si substrate to yield unstrained and strained-layer SLs, respectively (each has its uses). Figure 2 (a) shows a schematic cross-

sectional view of the SL structure deposited by precision MBE techniques. The overall thickness of the SL in the growth direction is typically 3-5 μm (about 200 layer pairs) to allow adequate absorption. The thicknesses of the individual layers, however, determine the optical properties. The lateral dimensions of the SL should appear to be at least λ , so that simple optical coupling can be used. (Note that Fig. 2 (a) is not to scale.) Figure 2 (b) shows the magnified cross-section of a superlattice made in 2001 at the UIC Microphysics Laboratory that shows excellent layer definition. (Dark spots are HgTe smearing likely caused by the sectioning process.)

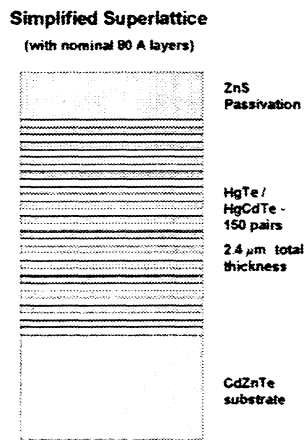


Figure 2 (a) - Schematic SL

TEM Image of HgTe/HgCdTe Superlattice

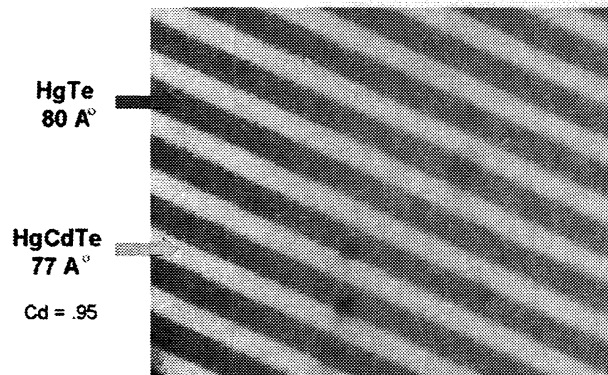


Figure 2 (b) - Actual SL

For detectors, superlattices have a number of advantages over alloy semiconductors:

- (a) the bandgap is easier to control because it depends on layer thickness rather than composition,
- (b) the large effective masses of electrons and holes in the growth direction lead to an order of magnitude (or more) reduction in tunneling currents,
- (c) carrier degeneracy effects (conduction band filling) near the long- λ band edge are less significant, and
- (d) a superlattice can suppress Auger recombination by intentionally inducing strain.

2.3 SL Design

The required thicknesses for the well (d_w) and barrier (d_b) layers of a SL are determined from band structure calculations, but can be summarized as follows. The band gap of a HgTe/CdTe superlattice depends almost entirely on the HgTe well thickness (d_w). because the barrier height of the semiconductor CdTe (or that of the Hg_{0.05}Cd_{0.95}Te actually used), is much greater than the well depth of the semi-metal HgTe. Typically a barrier thickness of 50 Å is used in order to allow “perpendicular”

charge transport, while maintaining a sufficiently large difference in the parallel and perpendicular effective masses. For temperatures $T < 40$ K, when d_w is < 62 Å, the SL is a semiconductor with a normal band structure with the E1 subband $>$ H1 subband. At approximately 62 Å the band gap E_g reduces to zero, and when $d_w > 62$ Å, the band structure is inverted (i.e., the H1 subband is now the conduction band). Absorption coefficients for the regular and inverted regions of the same gap are approximately the same. Noteworthy is the very weak dependence of E_g on the HgTe width, especially in the inverted gap region. Another interesting result is that whereas E_g for fixed d_w decreases with cooling in the normal bandgap region, it increases with cooling in the inverted region. Figures 3 illustrates this behavior graphically. Although we are interested in only the lowest subbands, which determine the long wavelength properties of the SL material, the higher order subbands (such as the L1-E1, etc.) dictate the optical properties at shorter wavelengths. This is quite convenient, because we can use readily available instrumentation at near- and mid-IR wavelengths to evaluate material properties relative to theoretical predictions. The material does not even need to be cooled. Full details on the band structure calculations may be found in C. Becker *et al* [8].

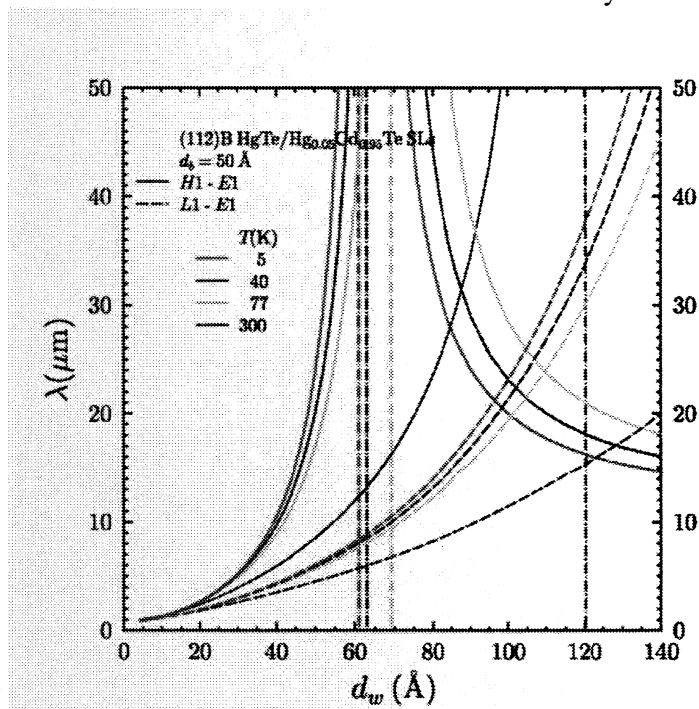


Figure 3 - Cutoff wavelength as a function of HgTe layer thickness. Inverted gap transitions are indicated by curves of negative slope. Vertical lines show thickness for zero gap at indicated temperature (from C. Becker *et al.* [8])

2.4 SL – Fabrication and Testing

The thickness required for the SL stack depends on the absorption coefficient of the material. Theoretical predictions, confirmed by FTIR absorption measurements at least in the mid-IR around 3-10 μm , indicate that the absorption coefficient at the H1-E1 band-edge is ~ 3000 cm^{-1} for $\lambda_c = 45$ μm SL material. A total SL thickness of 3 μm would therefore suffice for near unity internal quantum efficiency (compared to a thickness > 10 μm for a corresponding HgCdTe alloy). The calculations predict that the inverted band

region should have somewhat higher absorption than the normal band, although this point has yet to be verified experimentally.

A number of SL films were grown with various well depths to test the theoretical predictions for cut-off wavelength. To start we fabricated films for the mid-IR, because the wavelength response in the $\lambda = 3\text{-}20\ \mu\text{m}$ region is easy to measure with an available spectrometer. All the SL films grown at UIC are well characterized [9,10,11]. Crystal quality during growth is monitored through *in situ* spectroscopic ellipsometry and RHEED pattern techniques. The mechanical properties of the films are further investigated by x-ray diffraction and TEM measurements. Carrier mobility and concentration are measured by the Hall effect, while optical characteristics are determined by FTIR absorption and photoresponse spectra. The as-grown SL films usually have excellent mobilities around $3\times 10^4\ \text{cm}^2/\text{V}\cdot\text{s}$ to $1\times 10^5\ \text{cm}^2/\text{V}\cdot\text{s}$ at $T = 40\text{K}$, with the lower gap films having the higher mobility (as expected). All the SL material discussed here was grown n-type by introducing indium donors during the MBE growth process.

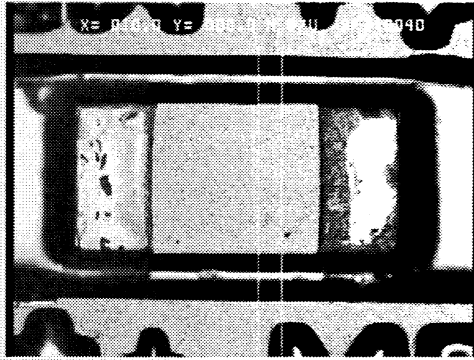
Finally, we should emphasize that two key tasks were accomplished regarding MBE growth of SL-based device structures. The first is the growth of multi-layer device structures with the SL-layers sandwiched between appropriately doped alloy layers with many graded hetero-interfaces. The structures were band-gap engineered to achieve good transport properties in the growth direction while suppressing tunneling currents. The second is the successful growth of SL structures on CdTe/Si substrates as well as lattice-matched CdZnTe substrates. MBE growth on CdTe/Si leads to a strained-layer SL that may be useful for suppressing Auger recombination.

3. Devices

3.1 Photoconductors

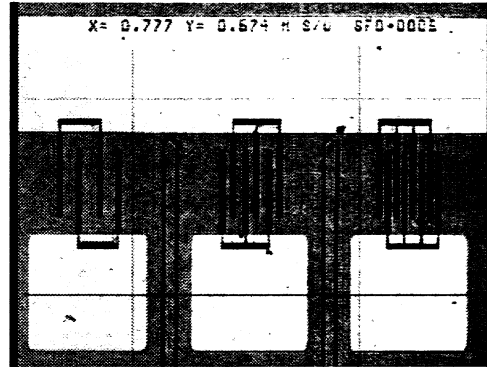
Once good quality SL films have been deposited, the easiest device to fabricate is the simple photoconductor (PC). Our first devices used conventional side contacts as shown in Figure 4a. Later an easier approach was adopted with top-surface interdigitated electrodes (IDE) as shown for three different electrode spacings in Figure 4b. The short inter-electrode spacing of the IDE devices leads to a fast transit time for carriers, and hence the broadest possible IF bandwidth when the device is used as a photomixer.

Superlattice Photoconductor



300 x 300 μm SL-PC with In+Au pads on HgTe/HgCdTe & Ti+Au on CdZnTe

(a)



(b)

Figure 4 - (a) Standard SL photoconductor (PC) with side contacts. (b) Three IDE style PC detectors with different electrode spacings. Active area per element is $200 \mu\text{m} \times 200 \mu\text{m}$ less regions blocked by electrodes. The light regions are electrode metalizations.

Figure 5 shows representative photoresponse spectra from two different SL materials. The peak intensity is defined by λ_p , while the -3 dB intensity is given by the cutoff wavelength λ_c on the long wavelength side. Spectra were measured at $T=77 \text{ K}$ using a Nicolet 870 FTIR which works out to $\lambda=25 \mu\text{m}$. The long wavelength limit of the FTIR will be upgraded to $\lambda=500 \mu\text{m}$ in the near future. As mentioned above, for our initial SL experiments it is much easier to work with wide bandgap materials, whose optical properties can be verified with standard mid-IR instrumentation. After we are certain that fabricated devices match theoretical predictions, we can be more confident in designing subsequent SL devices optimized for FIR wavelengths.

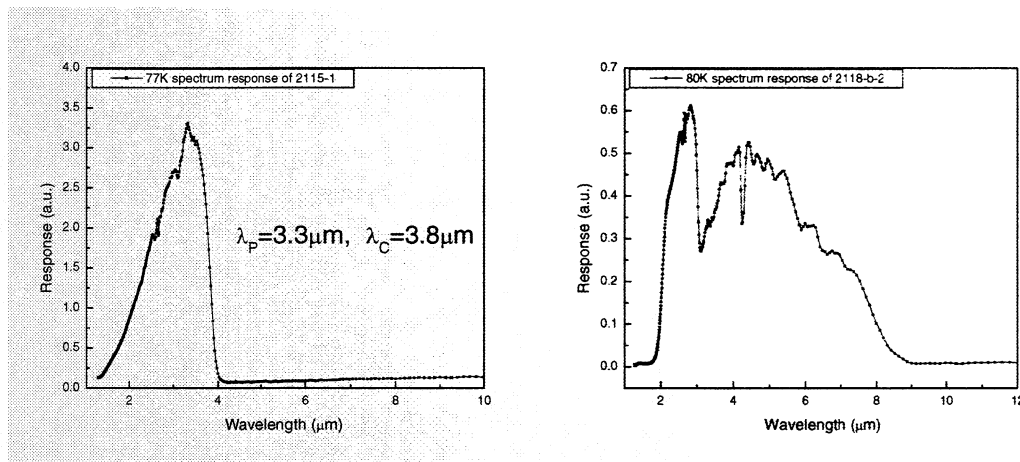


Figure 5 - (a) The 77 K relative spectral response of a $40 \mu\text{m} \times 40 \mu\text{m}$ device from SL2115 ($d_w=30 \text{ \AA}, d_b=26 \text{ \AA}$) with $\lambda_c=3.8 \mu\text{m}$ and (b) that of a $580 \mu\text{m} \times 580 \mu\text{m}$ device from SL2118 ($d_w=45 \text{ \AA}, d_b=25 \text{ \AA}$) with $\lambda_c=7.4 \mu\text{m}$.

3.2 Photodiodes

3.2.1 Standard process: p-type doping with As

Another device topology for photomixers is the reversed-biased photodiode (PD). The high field in the depletion region together with the short electrode spacing leads to a fast response time and high IF bandwidth. However, as the bandgap of the material is reduced toward zero, we must increasingly be concerned with tunneling currents. It remains to be seen whether PC or PD devices will prove superior as FIR mixers. The alloy and superlattice materials described above can be processed into photodiodes by the addition of a p-type layer onto the n-type material. The method currently favored for p-on-n in alloys is As-doping via ion implantation, although *in situ* As-doping during MBE material growth has also been used. Arsenic is favored here because of its relatively low thermal diffusion constant in HgCdTe. However, the As must be “activated” to occupy a Te site in the lattice if it is to function as an acceptor. This activation is readily accomplished by thermal annealing at $T = 250\text{-}300\text{ }^{\circ}\text{C}$ for 30-180 min. Although annealing causes no harm to alloy material, it is problematic for a SL which is itself grown at lower temperatures of $T=150\text{-}180\text{ }^{\circ}\text{C}$. To verify the deleterious effects of high temperatures on SL material, we ran a series of annealing experiments on samples from different SL batches. As expected, the $250\text{ }^{\circ}\text{C}$ anneal for 30 min caused noticeable interdiffusion between the SL layers, so much so that Hall mobilities dropped by a factor of 50 and the mid-IR absorption of the SL departed significantly from that measured for as-grown material. So now we must consider alternative methods for junction formation.

3.2.2 New Process: p-type doping with Au

Acceptors can also be introduced to II-VI compounds by substituting from the Group I elements (e.g., Li, Au, Ag, Cu). For p-type doping these elements would substitute for Hg or Cd in the lattice. Au is currently favored as an acceptor in II-VI heterostructures where the high temperature activation required by As is unacceptable. Au has a high thermal diffusivity, however, which needs to be controlled for good junction formation. The Microphysics Lab at UIC is currently working on p-type doping with Au under the Collaborative Alliance Technology program supported by the Army. Some preliminary, though encouraging, results have just been achieved with Au-doping to yield the first p-n junctions in a II-VI SL material. The junctions were formed by thermal diffusion of Au into n-type SL material at $110\text{ }^{\circ}\text{C}$, which is below the $180\text{ }^{\circ}\text{C}$ deposition temperature of the SL itself. The device structure is illustrated in Figure 6.

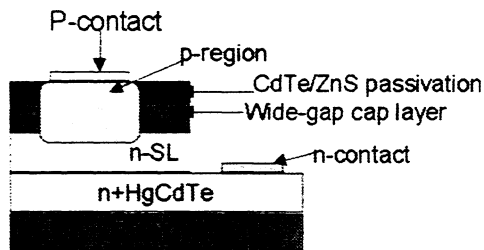


Figure 6 – Schematic cross-section of planar SL photodiode

Figure 7 shows the I/V curves of a junction grown on a sample of SL material. Although the R_0A values are far from the state of the art, they are quite encouraging for a first try. We believe improvements in the process technology will raise R_0A and detectivity closer to values achieved in alloys with As-doping. Our goal is not to compete with alloys, however, but to extend HgCdTe technology to the FIR where alloys are problematic. At this point - a little more than 2 years into the project - all the first-level technology challenges for SL-based photodiodes have already been met. However, much still needs to be done to realize the full potential of the device.

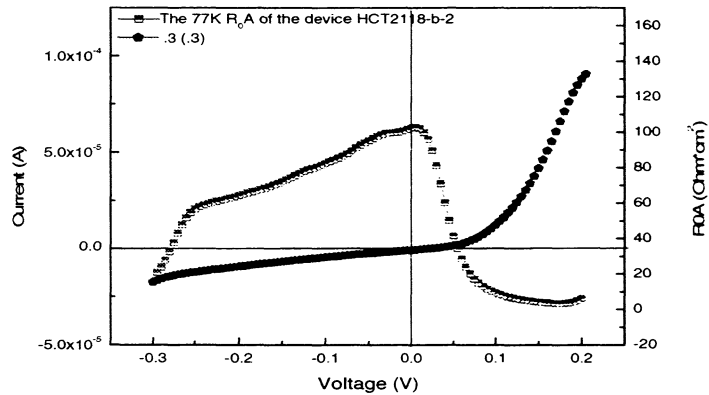


Figure 7 - The I-V and R_0A curves at $T=77K$ for a $580 \mu\text{m} \times 580 \mu\text{m}$ photodiode made from material SL-2118 with $\lambda_c=7.4 \mu\text{m}$ (see Fig. 5b).

Now that we can make SL devices, we are starting to test the speed of selected mid-IR detectors with IDE contacts. This is done by measuring the spectrum of the G-R noise power, which corresponds roughly to the expected IF bandwidth. Our goal is an IF bandwidth exceeding 3 GHz in a FIR device. Simultaneously, we are fabricating new SL materials with bandgaps closer to zero, so that FIR measurements can be started.

This work is supported by NASA Grant NAG5-10213.

References

- [1] E.E. Haller and J.W. Beeman, "Far Infrared Photoconductors: Recent Advances and Future Prospects", in Proc. Far-IR, Sub-mm, & Millimeter Detector Technology Workshop, J. Wolf, J. Farhoomand, and C.R. McCreight (eds.), NASA CP-211408 (2002), paper 2-06
- [2] M. S. Sherwin, C. Cates, B. Serapiglia, Y. Dora, J. B. Williams, K. Maranowski, A.C. Gossard, and W. R. McGrath, "Tunable Antenna-Coupled Intersubband (TACIT) Mixers: The Quantum Limit without the Quantum Liquid", in Proc. Far-IR, Sub-mm, & Millimeter Detector Technology Workshop, J. Wolf, J. Farhoomand, and C.R. McCreight (eds.), NASA CP-211408 (2002), paper 6-03

- [3] S. V. Bandara, S. D. Gunapala, D. Z-Y. Ting, S. B. Rafol, and J. K. Liu, "GaAs/AlGaAs Multi-Quantum-Well Based Far Infrared Detectors for Astronomy", in Proc. Far-IR, Sub-mm, & Millimeter Detector Technology Workshop, J. Wolf, J. Farhoomand, and C.R. McCreight (eds.), NASA CP-211408 (2002), paper 6-06
- [4] A.L. Betz, R.T. Boreiko, S. Sivananthan, and Y.D. Zhou, "Far-Infrared Focal Plane Arrays", in Proc. Far-IR, Sub-mm, & Millimeter Detector Technology Workshop, J. Wolf, J. Farhoomand, and C.R. McCreight (eds.), NASA CP-211408 (2002), paper 6-07
- [5] A.L. Betz and R.T. Boreiko, "Space Applications for HgCdTe at FIR Wavelengths Between 50-150 μm ", in *Materials for Infrared Detectors*, R.E. Longshore (ed.), Proc. SPIE Vol. 4454, pp. 1-9 (2001)
- [6] A.L. Betz, R.T. Boreiko, S. Sivananthan, and R. Ashokan, "HgCdTe Photoconductive Mixers for 2-8 THz", in Proc. 12th International Symposium on Space Terahertz Technology (JPL Publ. 01-18), pp. 92-101 (2001)
- [7] G.L. Hanson, and J.L. Schmit, Jour. Appl. Phys., **54**, 1639 (1983)
- [8] C.R. Becker, V. Latussek, G. Landwehr, and L.W. Molenkamp, "Inverted band structure of type III HgTe/Hg_{1-x}Cd_xTe superlattices and its temperature dependence", Phys. Rev. B, **68**, 035202 (2003)
- [9] Y.D. Zhou, C.R. Becker, R. Ashokan, Y. Selamet, Y. Chang, R.T. Boreiko, A.L. Betz, S. Sivananthan, "Progress in Far-Infrared Detection Technology", Proc. SPIE Volume 4795, p. 121 (2002)
- [10] Y.D. Zhou, C.R. Becker, Y. Selamet, Y. Chang, J. Zhao, R. Ashokan, R.T. Boreiko, T. Aoki, D.J. Smith, A.L. Betz, S. Sivananthan, "Far-infrared Detector Based on HgTe/HgCdTe Superlattices", Proc. II-VI MCT Workshop, San Diego (2002).
- [11] Y.D. Zhou, J. Zhao, R.T. Boreiko, Y. Selamet, Y. Chang, R. Ashokan, C. Bucker, A.L. Betz, S. Sivananthan, "HgCdTe for far-infrared heterodyne detection", SPIE Proc. (2003, submitted)